



**HAL**  
open science

# An Eulerian Approach for Simulating Frictional Heating in Disc-Pad Systems

Niclas Stromberg

► **To cite this version:**

Niclas Stromberg. An Eulerian Approach for Simulating Frictional Heating in Disc-Pad Systems. European Journal of Mechanics - A/Solids, 2011, 30 (5), pp.673. 10.1016/j.euromechsol.2011.04.004 . hal-00769684

**HAL Id: hal-00769684**

**<https://hal.science/hal-00769684>**

Submitted on 3 Jan 2013

**HAL** is a multi-disciplinary open access archive for the deposit and dissemination of scientific research documents, whether they are published or not. The documents may come from teaching and research institutions in France or abroad, or from public or private research centers.

L'archive ouverte pluridisciplinaire **HAL**, est destinée au dépôt et à la diffusion de documents scientifiques de niveau recherche, publiés ou non, émanant des établissements d'enseignement et de recherche français ou étrangers, des laboratoires publics ou privés.

# Accepted Manuscript

Title: An Eulerian Approach for Simulating Frictional Heating in Disc-Pad Systems

Authors: Niclas Stromberg

PII: S0997-7538(11)00050-7

DOI: [10.1016/j.euromechsol.2011.04.004](https://doi.org/10.1016/j.euromechsol.2011.04.004)

Reference: EJMSOL 2702

To appear in: *European Journal of Mechanics / A Solids*

Received Date: 2 March 2011

Revised Date: 12 April 2011

Accepted Date: 15 April 2011

Please cite this article as: Stromberg, N. An Eulerian Approach for Simulating Frictional Heating in Disc-Pad Systems, *European Journal of Mechanics / A Solids* (2011), doi: 10.1016/j.euromechsol.2011.04.004

This is a PDF file of an unedited manuscript that has been accepted for publication. As a service to our customers we are providing this early version of the manuscript. The manuscript will undergo copyediting, typesetting, and review of the resulting proof before it is published in its final form. Please note that during the production process errors may be discovered which could affect the content, and all legal disclaimers that apply to the journal pertain.



# An Eulerian Approach for Simulating Frictional Heating in Disc-Pad Systems (revised version)

Niclas Strömberg

Department of Mechanical Engineering  
Jönköping University  
SE-551 11 Jönköping, Sweden  
E-mail: niclas.stromberg@jth.hj.se

April 12, 2011

## Abstract

*Thermal stresses as a result from frictional heating must be considered when designing disc brakes, clutches or other rotating machine components with sliding contact conditions. The rotational symmetry of the disc in these kind of applications makes it possible to model these systems using an Eulerian approach instead of a Lagrangian framework. In this paper such an approach is developed and implemented. The disc is formulated in an Eulerian frame where the convective terms are defined by the angular velocity. By utilizing the Eulerian framework, a node-to-node formulation of the contact interface is obtained, producing most accurate frictional heat power solutions. The energy balance of the interface is postulated by introducing an interfacial temperature. Both frictional power and contact conductances are included in this energy balance. The contact problem is solved by a non-smooth Newton method. By adopting the augmented Lagrangian approach, this is done by rewriting Signorini's contact conditions to an equivalent semi-smooth equation. The heat transfer in the disc is discretized by a Petrov-Galerkin approach, i.e. the numerical difficulties due to the non-symmetric convective matrix appearing in a pure Galerkin discretization is treated by following the streamline-upwind approach. In such*

*manner a stabilization is obtained by adding artificial conduction along the streamlines. For each time step the thermoelastic contact problem is first solved for the temperature field from the previous time step. Then, the heat transfer problem is solved for the corresponding frictional power. In such manner a temperature history is obtained sequentially via the trapezoidal rule. In particular the parameter is set such that both the Crank-Nicolson and the Galerkin methods are utilized. The method seems very promising. This is demonstrated by solving a two-dimensional benchmark as well as a real disc brake system in three dimension.*

**Keywords:** Eulerian framework, frictional heat, hot spots, heat bands

## 1 Introduction

In this paper an Eulerian approach for rotating thermo-mechanical systems with frictional heating is developed. In the design of machine components like brakes and clutches it is of importance to consider effects from frictional heating. Today, this is mostly done by experiments. The Lagrangian approaches in our commercial finite element softwares usually fail due to convergence difficulties in the contact algorithms or because of too long computational times. An idea to improve these draw-backs is to formulate the problem in an Eulerian frame instead. This is the topic of the following paper.

Previously, we have studied thermo-mechanical contact problems in the setting of small displacements. In Strömberg [1] thermo-mechanical wear problems were studied for a thermo-elastic body in unilateral contact with a rigid foundation. The development of hot spots was studied by solving the fully coupled equation system by using Newton's method. The influence of wear on these hot spots was also investigated numerically. That work was later extended to the case of two thermo-elastic bodies in unilateral contact [2]. An even earlier work on this topic from the same research group can be found in [3]. **The paper by Zavarise et al. [4] is another example of early works by other researchers on this topic.**

In the following paper, the thermo-mechanical framework developed in our previous works is now extended to also include large rotations with superimposed small displacements and this is done in an Eulerian framework. Previously, we have studied mechanical systems using similar frameworks. In Klarbring et al. [5], the transmission error in a spur gear system was studied by superimposing small displacements on

rigid body motions. That approach is now extended such that thermal effects are also included.

Examples of early works on frictional heating in large displacements are e.g. the papers by **Wriggers and Miehe [6]**, Oancea and Laursen [7], and by Agelet de Saracibar [8]. A more recent paper is the one by Rieger and Wriggers [9] where the accuracy of the contact solution, which is most important in order to represent the frictional power sufficiently well, was controlled by adaptive techniques. Another way to improve the contact solution in large displacements is to use the mortar technique. This technique has lately become very popular for treating non-matching meshes in contact problems, see e.g. [10, 11] Recently, the mortar approach was investigated by Hübner and Wohlmuth [12] for thermo-mechanical friction problems. A nice feature with the presented Eulerian approach in this paper is that the contact region is always well defined and a node-to-node based approach can be adopted, producing most accurate contact solutions. The contact equations are then treated with the celebrated augmented Lagrangian approach (see e.g. the original work by Alart and Curnier [13]), where the corresponding equation system is solved by a non-smooth Newton algorithm. The details can be found in Strömberg [14]. This Newton approach has been utilized in number of works for solving non-smooth and non-linear mechanical and thermo-mechanical problems. Most recently it was used by Strömberg [15] for performing topology optimization of design domains with contact constraints.

One can find several other works where a Lagrangian formulation has been utilized for treating frictional heating, see e.g. [16], but it is not so easy to find papers on **thermo-mechanical** finite element analysis where Eulerian frameworks are used. Recently, one such paper was presented by Wauer and Schweizer [17]. They considered a rotating thermo-elastic disc with a stationary heat source using convective heat transfer. Thus, the frictional heat was not obtained by any contact analysis as is done in the present paper. Non-finite element analyzes by using Eulerian frameworks on this topic seem to appear more frequently in the litterature. One example is the paper by Pauk and Yevtushenko [18] where a cylinder sliding over a half-space was considered. In another paper, Yevtushenko et al. [19] considered frictional heating between a pin and a rotating disc. This problem was also studied by Laraqi et al. [20]. **Of course, finite element analyzes of mechanical contact problem by using Eulerian approaches appear more frequently, see e.g. the paper by Nackenhorst [21] where an arbitrary Lagrangian Eulerian formulation for rolling contact is proposed.**

In this paper we present a finite element approach using an Eulerian

framework for solving frictional heating in rotating systems such as disc-pad systems. The fully coupled problem is decoupled in one mechanical part and another thermal problem. These two equation systems are then solved sequentially by using Crank-Nicolson's or Galerkin's settings of the trapezoidal rule for the time discretization. Other possibilities of performing the time discretization are of course also available. For instance, Laursen [22] proposed thermodynamically consistent algorithms for this class of problems. The convective term is stabilized by the streamline-upwind approach. For this task the excellent text-book by Donea and Huerta [23] has been consulted.

The proposed method is implemented on 64-bits Windows using Intel Fortran, and the sparse Cholesky and LU solvers of Matlab. The pre- and postprocessing are performed by using Abaqus/CAE through Python scripts. The implementation seems to be very robust and produce accurate solutions at low computational times. This is demonstrated by presenting numerical examples in both 2D and 3D.

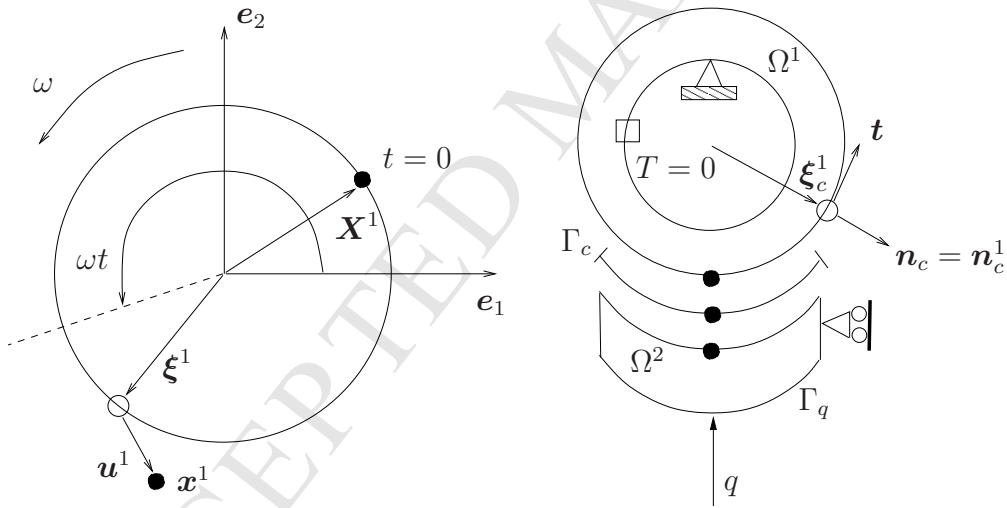


Figure 1: A rotating disc and a pad in sliding contact. The motion of the disc is governed by a prescribed rigid body rotation  $\xi^1$  and superimposed small displacements  $\mathbf{u}^1$ .

## 2 Governing equations

Let us consider a rotating disc ( $\Omega^1$ ) and a pad ( $\Omega^2$ ) subjected to an external pressure  $q$  on a boundary  $\Gamma_q$  of the pad as shown in Figure 1.

The disc is rotating with a constant angular velocity  $\omega$ . At a time  $t$ , the **spatial** position  $\boldsymbol{x}^1$  of a **material** point  $\boldsymbol{X}^1$  on the disc is given by a rigid body rotation

$$\boldsymbol{\xi}^1 = \boldsymbol{\xi}(\boldsymbol{X}^1, t) = \boldsymbol{Q}(t)\boldsymbol{X}^1, \quad (1)$$

where

$$\boldsymbol{Q} = \boldsymbol{Q}(t) = \begin{bmatrix} \cos(\omega t) & -\sin(\omega t) & 0 \\ \sin(\omega t) & \cos(\omega t) & 0 \\ 0 & 0 & 1 \end{bmatrix}, \quad (2)$$

and superimposed small displacements  $\boldsymbol{u}^1 = \boldsymbol{u}(\boldsymbol{\xi}^1, t)$ . That is, the position of  $\boldsymbol{X}^1$  is given by

$$\boldsymbol{x}^1 = \boldsymbol{x}(\boldsymbol{X}^1, t) = \boldsymbol{Q}(t)\boldsymbol{X}^1 + \boldsymbol{u}(\boldsymbol{\xi}(\boldsymbol{X}^1, t), t). \quad (3)$$

The motion of the pad is only governed by small displacements  $\boldsymbol{u}(\boldsymbol{X}^2, t)$  such that the position  $\boldsymbol{x}^2 = \boldsymbol{x}(\boldsymbol{X}^2, t)$  of a point  $\boldsymbol{X}^2$  on the pad can be considered to coincide with  $\boldsymbol{X}^2$ , i.e.  $\boldsymbol{x}^2 \approx \boldsymbol{X}^2$ . Of course, due to the assumption of superimposed small displacements for the disc, we also have that  $\boldsymbol{x}^1 \approx \boldsymbol{\xi}^1$ . Thus, the displacement at the position  $\boldsymbol{\xi}^1$  shown in Figure 1 is exaggerated in order to improve the illustration of the kinematics.

The velocity of a material point  $\boldsymbol{X}^1$  passing a spatial position  $\boldsymbol{\xi}^1$  on the disc is obtained by taking the material time derivative of (3) and using  $\boldsymbol{X}^1 = \boldsymbol{Q}^T \boldsymbol{\xi}^1$  from (1), i.e.

$$\boldsymbol{v}^1 = \boldsymbol{v}(\boldsymbol{\xi}^1, t) = \dot{\boldsymbol{x}}^1 = \dot{\boldsymbol{Q}}\boldsymbol{X}^1 + \dot{\boldsymbol{u}}(\boldsymbol{\xi}^1, t) = \dot{\boldsymbol{Q}}\boldsymbol{Q}^T \boldsymbol{\xi}^1 + \dot{\boldsymbol{u}}(\boldsymbol{\xi}^1, t) \quad (4)$$

or

$$\boldsymbol{v}^1 = \boldsymbol{\omega} \times \boldsymbol{\xi}^1 + \dot{\boldsymbol{u}}(\boldsymbol{\xi}^1, t), \quad (5)$$

where  $\boldsymbol{\omega} = \omega \boldsymbol{e}_3$  is the axial vector of  $\dot{\boldsymbol{Q}}\boldsymbol{Q}^T$ . In the following development, it will be assumed that the latter term in (5) is negligible such that  $\boldsymbol{v}^1 = \boldsymbol{\omega} \times \boldsymbol{\xi}^1$  can be used for the disc.

A common contact interface  $\Gamma_c$  is identified for the two bodies, which in turn defines the contact surface  $\Gamma_c^m$  ( $m = 1, 2$ ) of respectively body  $\Omega^m$ . This is done in such manner that for each point  $\boldsymbol{x}_c^2 \approx \boldsymbol{X}_c^2$  on  $\Gamma_c^2$  we identify a unique **spatial position**  $\boldsymbol{\xi}_c^1 = \boldsymbol{\xi}(\boldsymbol{X}_c^1, t)$  on  $\Gamma_c^1$ .  $\boldsymbol{X}_c^2$  and the corresponding  $\boldsymbol{\xi}_c^1$  define together a unique contact pair. At every time  $t$  we assume that  $\boldsymbol{\xi}(\boldsymbol{X}_c^1, t) = \boldsymbol{X}_c^2$  is satisfied for all such unique contact pairs. Thus, for  $\omega > 0$ , a new material point  $\boldsymbol{X}_c^1$  will come in contact at the spatial position  $\boldsymbol{\xi}_c^1$  with  $\boldsymbol{X}_c^2$  continuously.

The relative displacement for a contact pair is defined by

$$\boldsymbol{\delta} = \boldsymbol{x}_c^1 - \boldsymbol{x}_c^2. \quad (6)$$

By inserting (1) and (3), and using  $\mathbf{x}_c^2 = \mathbf{X}_c^2 + \mathbf{u}(\mathbf{X}_c^2, t)$ , this definition becomes

$$\boldsymbol{\delta} = \boldsymbol{\xi}_c^1 - \mathbf{X}_c^2 + \mathbf{u}(\boldsymbol{\xi}_c^1, t) - \mathbf{u}(\mathbf{X}_c^2, t). \quad (7)$$

For a well defined contact pair we have  $\boldsymbol{\xi}_c^1 = \mathbf{X}_c^2$ , implying that the two first terms will cancel out and we obtain  $\boldsymbol{\delta} = \mathbf{u}(\boldsymbol{\xi}_c^1, t) - \mathbf{u}(\mathbf{X}_c^2, t)$ . This is one of the key features of the proposed Eulerian approach.

The relative displacement in the normal direction<sup>1</sup> is obtained by

$$\delta_n = \boldsymbol{\delta} \cdot \mathbf{n}_c, \quad (8)$$

where

$$\mathbf{n}_c = \mathbf{n}_c^1 = \frac{\boldsymbol{\xi}_c^1}{|\boldsymbol{\xi}_c^1|}. \quad (9)$$

We also have that the outward unit normal direction  $\mathbf{n}_c^2 = -\mathbf{n}_c$  on  $\Gamma_c^2$ , since  $\Gamma_c^1 = \Gamma_c^2$ .

By taking the material time derivative of (7) gives us the relative velocity

$$\dot{\boldsymbol{\delta}} = \boldsymbol{\omega} \times \boldsymbol{\xi}_c^1 + \dot{\mathbf{u}}(\boldsymbol{\xi}_c^1, t) - \dot{\mathbf{u}}(\mathbf{X}_c^2, t). \quad (10)$$

In the following it is assumed that the two latter terms can be neglected such that  $\dot{\boldsymbol{\delta}} = v_c \mathbf{t}$ , where

$$v_c = |\boldsymbol{\omega} \times \boldsymbol{\xi}_c^1| = |\boldsymbol{\xi}_c^1| \omega \quad \text{and} \quad \mathbf{t} = \frac{\boldsymbol{\omega} \times \boldsymbol{\xi}_c^1}{|\boldsymbol{\omega} \times \boldsymbol{\xi}_c^1|}. \quad (11)$$

By introducing Cauchy's stress  $\boldsymbol{\sigma}$  and assuming no body forces, the balance in momentum is represented for each body by the equation of motion in the following manner:

$$\frac{\partial \sigma_{ij}}{\partial x_j} = \rho \ddot{x}_i \quad \text{in } \Omega^m \quad (m = 1, 2), \quad (12)$$

where  $\rho$  is the density of mass. Taking the material time derivative of (5) and using the assumption  $\dot{\boldsymbol{\omega}} = 0$  imply that

$$\ddot{\mathbf{x}} = \boldsymbol{\omega} \times \boldsymbol{\xi}_c^1 + \ddot{\mathbf{u}}(\boldsymbol{\xi}_c^1, t) = \boldsymbol{\omega} \times (\boldsymbol{\omega} \times \boldsymbol{\xi}_c^1) + \ddot{\mathbf{u}}(\boldsymbol{\xi}_c^1, t) \quad \text{in } \Omega^1. \quad (13)$$

We now assume that the latter term is negligible such that  $\ddot{\mathbf{x}} = -\omega^2 \boldsymbol{\xi}_c^1$  can be used for  $\Omega^1$ . Furthermore, we also assume that the inertia term

---

<sup>1</sup>For the three-dimensional disc considered in the numerical examples we let  $\mathbf{n}_c = \mathbf{e}_3$ .

$\rho\ddot{\mathbf{u}}(\mathbf{X}, t)$  is so small that it can be neglected for  $\mathbf{X} \in \Omega^2$ . Then, (12) can be written as

$$\frac{\partial \sigma_{ij}}{\partial x_j} = -\rho\omega^2 \xi_i \quad \text{in } \Omega^1, \quad (14a)$$

$$\frac{\partial \sigma_{ij}}{\partial x_j} = 0 \quad \text{in } \Omega^2. \quad (14b)$$

In addition, boundary conditions such as

$$\boldsymbol{\sigma} \mathbf{n}_q = -q \mathbf{n}_q \quad \text{on } \Gamma_q, \quad (15)$$

where  $\mathbf{n}_q$  is a outward unit normal direction on  $\Gamma_q$ , are also satisfied together with boundary conditions on  $\mathbf{u}$  and  $T$ . In particular, the boundary conditions on  $\Gamma_c^m$  are treated by defining a contact traction vector  $\mathbf{p}$  in the following way:

$$\mathbf{p} = -\boldsymbol{\sigma} \mathbf{n}_c \quad \text{on } \Gamma_c^1. \quad (16)$$

The principle of action and reaction then implies that

$$\boldsymbol{\sigma} \mathbf{n}_c^2 = \mathbf{p} \quad \text{on } \Gamma_c^2. \quad (17)$$

The contact traction vector is also decomposed into the normal contact pressure

$$p_n = \mathbf{p} \cdot \mathbf{n}_c \quad (18)$$

and the tangential component

$$p_t = \mathbf{p} \cdot \mathbf{t}, \quad (19)$$

such that  $\mathbf{p} = p_n \mathbf{n}_c + p_t \mathbf{t}$ .

The energy balance for each body is represented by

$$\rho c \dot{T} = k \sum_{i=1}^3 \frac{\partial^2 T}{\partial x_i^2}, \quad (20)$$

respectively, where  $c$  is the specific heat capacity and  $k$  is the thermal conductivity. The temperature  $T$  of the disc  $\Omega^1$  is considered to be a function of the position vector  $\boldsymbol{\xi}$ , i.e.  $T = T(\boldsymbol{\xi}, t)$ . Thus,

$$\dot{T} = \frac{\partial T}{\partial t} + \frac{\partial T}{\partial \xi_i} \dot{\xi}_i = \frac{\partial T}{\partial t} + (\boldsymbol{\omega} \times \boldsymbol{\xi})_i \frac{\partial T}{\partial \xi_i}. \quad (21)$$

Consequently, the energy balance for the first body also reads

$$\rho c \frac{\partial T}{\partial t} + \rho c (\boldsymbol{\omega} \times \boldsymbol{\xi})_i \frac{\partial T}{\partial \xi_i} = k \sum_{i=1}^3 \frac{\partial^2 T}{\partial x_i^2}. \quad (22)$$

The energy balance for the contact interface  $\Gamma_c$  is written as

$$p_t v_c + \mathbf{q}^1 \cdot \mathbf{n}_c^1 + \mathbf{q}^2 \cdot \mathbf{n}_c^2 = 0, \quad (23)$$

postulating that the total heat transfer must balance the frictional heat power generated on  $\Gamma_c$ . Here,  $\mathbf{q}^m$  represents the heat flux vector in each body  $\Omega^m$ , respectively. One should be aware that constitutive assumptions, such as e.g. Fourier's law of heat transfer and zero heat capacity of the contact interface  $\Gamma_c$ , are needed to derive the balance laws postulated in (20) and (23) by starting from the first principle of thermodynamics. A detailed derivation of these balance laws can be found in Strömberg [1].

Linear thermo-elasticity is adopted for the bodies, i.e. the Cauchy stress is governed by

$$\sigma_{ij} = \lambda \epsilon_{kk} \delta_{ij} + 2G \epsilon_{ij} - (3\lambda + 2G) \alpha T \delta_{ij}, \quad (24)$$

where

$$\epsilon_{ij} = \frac{1}{2} \left( \frac{\partial u_i}{\partial x_j} + \frac{\partial u_j}{\partial x_i} \right) \quad (25)$$

is the engineering strain,  $\lambda$  and  $G$  are Lamé's coefficients, and  $\alpha$  is the thermal dilatation coefficient. In addition, an assumption of setting the reference temperature equal to zero is made in (24). Notice also that

$$\frac{\partial}{\partial x_i} = \frac{\partial}{\partial \xi_i} \quad (26)$$

in the disc, due to the assumption of small displacements.

Signorini's contact conditions are adopted for the contact interface. The normal displacement  $\delta_n$  must always be less or equal to zero. Otherwise, the disc will penetrate the pad which of course is impossible. No adhesive normal contact pressure is considered, and compressive normal contact pressure  $p_n > 0$  is only developed when the bodies are in contact. This is formulated by Signorini's contact conditions as

$$p_n \geq 0, \quad \delta_n \leq 0, \quad p_n \delta_n = 0. \quad (27)$$

An equivalent relationship of (27), which is used in the numerical treatment, reads

$$p_n = \frac{p_n + r\delta_n + |p_n + r\delta_n|}{2}, \quad (28)$$

where  $r > 0$  is any real number. This is the well-known projection<sup>2</sup> adopted in the augmented Lagrangian approach, see e.g. Strömberg [14].

<sup>2</sup>This is also frequently written as  $\min(p_n, -r\delta_n) = 0$ , see e.g. [24].

It is assumed that global sliding is always developed. Therefore, by following Coulomb, we set  $p_t = \mu p_n$ , where  $\mu$  is the friction coefficient. By inserting this into (23), the energy balance at the contact interface reads

$$\mu p_n v_c + \mathbf{q}^1 \cdot \mathbf{n}_c^1 + \mathbf{q}^2 \cdot \mathbf{n}_c^2 = 0, \quad (29)$$

Finally, we let the thermal contact conditions be governed by

$$\mathbf{q}^m \cdot \mathbf{n}_c^m = \varphi^m p_n (T^m - \mathcal{T}) \quad (m = 1, 2), \quad (30)$$

where  $\varphi^m$  are contact conductance coefficients for respectively contact surface and  $\mathcal{T}$  is an intrinsic temperature of  $\Gamma_c$ . Thus, it is assumed that the conductance at the contact interface depends linearly on the contact pressure, see also (34) which is derived below. By inserting (30) into the energy balance in (29), one can derive

$$\mathbf{q}^1 \cdot \mathbf{n}_c^1 = \frac{\varphi^1 \varphi^2}{\varphi^1 + \varphi^2} p_n (T^1 - T^2) - \frac{\varphi^1}{\varphi^1 + \varphi^2} \mu p_n v_c, \quad (31a)$$

$$\mathbf{q}^2 \cdot \mathbf{n}_c^2 = \frac{\varphi^1 \varphi^2}{\varphi^1 + \varphi^2} p_n (T^2 - T^1) - \frac{\varphi^2}{\varphi^1 + \varphi^2} \mu p_n v_c. \quad (31b)$$

In these relationships,

$$\varphi^0 = \frac{\varphi^1 \varphi^2}{\varphi^1 + \varphi^2} \quad (32)$$

represents the overall contact conductance, whereas

$$\xi_\mu^m = \frac{\varphi^m}{\varphi^1 + \varphi^2} \quad (33)$$

represents factors on how the frictional dissipation is divided between the contact interface and the contact surfaces, respectively. Thus, (31) can also be written as

$$\mathbf{q}^1 \cdot \mathbf{n}_c^1 = \varphi^0 p_n (T^1 - T^2) - \xi_\mu^1 \mu p_n v_c, \quad (34a)$$

$$\mathbf{q}^2 \cdot \mathbf{n}_c^2 = \varphi^0 p_n (T^2 - T^1) - (1 - \xi_\mu^1) \mu p_n v_c, \quad (34b)$$

since  $\xi_\mu^1 + \xi_\mu^2 = 1$ .

### 3 Finite element equations

The governing equations presented in the previous section are put together to equivalent weak formulations. These weak formulations are discretized by finite element approximations. The obtained finite element equations are summarized in this section.

The nodal displacements  $d_i^A = d_i^A(t)$  and the nodal temperatures  $T^A = T^A(t)$  are collected in  $\mathbf{d} = \mathbf{d}(t)$  and  $\mathbf{T} = \mathbf{T}(t)$ , respectively. Thus, the displacement  $\mathbf{u}$  and the temperature  $T$  are approximated accordingly to

$$u_i(\mathbf{x}, t) = \sum_{A=1}^{n_n} N^A(\mathbf{x}) d_i^A(t), \quad (35a)$$

$$T(\mathbf{x}, t) = \sum_{A=1}^{n_n} N^A(\mathbf{x}) T^A(t), \quad (35b)$$

where  $N^A = N^A(\mathbf{x})$  represents the shape functions, and  $n_n$  is the number of finite element nodes. We also arrange  $\mathbf{d}$  and  $\mathbf{T}$  in the following way:

$$\mathbf{d} = \left\{ \begin{array}{c} \mathbf{d}_1 \\ \mathbf{d}_2 \end{array} \right\}, \quad \mathbf{T} = \left\{ \begin{array}{c} \mathbf{T}_1 \\ \mathbf{T}_2 \end{array} \right\}, \quad (36)$$

such that  $\mathbf{d}_m$  and  $\mathbf{T}_m$  belong to respectively body  $\Omega^m$ .

At the contact surface of each body, the normal displacements at the finite element nodes are obtained by  $\mathbf{C}_{nm}\mathbf{d}_m$ , where the rows of the transformation matrices  $\mathbf{C}_{nm}$  contain surface normals  $\mathbf{n}_c^A$  in proper positions, i.e.

$$\mathbf{C}_{n1}^A = [\mathbf{0} (\mathbf{n}_c^A)^T \mathbf{0}], \quad (37a)$$

$$\mathbf{C}_{n2}^A = [\mathbf{0} (-\mathbf{n}_c^A)^T \mathbf{0}]. \quad (37b)$$

Of course, the relative normal displacement for all contact pairs can now be collected as

$$\boldsymbol{\delta}_n = \mathbf{C}_{n1}\mathbf{d}_1 + \mathbf{C}_{n2}\mathbf{d}_2. \quad (38)$$

The normal contact forces  $P_n^A$  at the finite element nodes on  $\Gamma_c$  are collected in  $\mathbf{P}_n$ . The discretization of (28) then reads

$$\mathbf{P}_n = \frac{\mathbf{P}_n + r\boldsymbol{\delta}_n + |\mathbf{P}_n + r\boldsymbol{\delta}_n|}{2}. \quad (39)$$

The finite element approximations of the equation of motion in (14) become

$$\mathbf{K}_1\mathbf{d}_1 - \hat{\mathbf{K}}_1\mathbf{T}_1 + (\mathbf{C}_{n1} + \mu\mathbf{C}_{t1})^T \mathbf{P}_n = \mathbf{F}_\omega, \quad (40a)$$

$$\mathbf{K}_2\mathbf{d}_2 - \hat{\mathbf{K}}_2\mathbf{T}_2 + (\mathbf{C}_{n2} + \mu\mathbf{C}_{t2})^T \mathbf{P}_n = \mathbf{F}_q, \quad (40b)$$

where  $E_{ijkl} = \lambda\delta_{ij}\delta_{kl} + G(\delta_{ik}\delta_{jl} + \delta_{il}\delta_{jk})$ ,

$$\mathbf{K}_m = [K_{ik}^{BA}], \quad K_{ik}^{BA} = \int_{\Omega^m} E_{ijkl} \frac{\partial N^A}{\partial x_l} \frac{\partial N^B}{\partial x_j} dV, \quad (41a)$$

$$\hat{\mathbf{K}}_m = [\hat{K}_i^{BA}], \quad \hat{K}_i^{BA} = \int_{\Omega^m} \alpha(3\lambda + 2G)N^A \frac{\partial N^B}{\partial x_i} dV, \quad (41b)$$

$$\mathbf{C}_{tm} = [\mathbf{C}_{tm}^A], \quad \mathbf{C}_{tm}^A = [\mathbf{0}(-1)^{m+1}\mathbf{t}^A \mathbf{0}], \quad (41c)$$

$$\mathbf{F}_\omega = \{F_{\omega i}^A\}, \quad F_{\omega i}^A = \omega^1 \int_{\Omega^1} \rho \xi_i N^A dV, \quad (41d)$$

$$\mathbf{F}_q = \{F_{qi}^A\}, \quad F_{qi}^A = - \int_{\Gamma_q} q n_{qi} N^A dA. \quad (41e)$$

From (32) we obtain that the heat power supply to the contact nodes on  $\Gamma_c^m$  can be written as

$$\mathbf{Q}_{c1} = \mathbf{Q}_{c1}(\mathbf{T}, \mathbf{P}_n) = \vartheta^0 \mathbf{P}_n \circ (\mathbf{S}_2 \mathbf{T}_2 - \mathbf{S}_1 \mathbf{T}_1) + \xi_\mu^1 \mu \mathbf{P}_n R_{\text{disc}} \omega, \quad (42a)$$

$$\mathbf{Q}_{c2} = \mathbf{Q}_{c2}(\mathbf{T}, \mathbf{P}_n) = \vartheta^0 \mathbf{P}_n \circ (\mathbf{S}_1 \mathbf{T}_1 - \mathbf{S}_2 \mathbf{T}_2) + (1 - \xi_\mu^1) \mu \mathbf{P}_n R_{\text{disc}} \omega, \quad (42b)$$

where  $\circ$  represents the Hadamard product and  $R_{\text{disc}} = |\boldsymbol{\xi}_c^1|$  is the outer radius of the disc. We have also introduced transformation matrices  $\mathbf{S}_m = [\mathbf{S}_m^A]$ , where  $\mathbf{S}_m^A = [\mathbf{0} [1] \mathbf{0}]$ , in order to obtain the correct nodal temperatures at the contact surfaces  $\Gamma_c^m$  from  $\mathbf{T}_m$ .

By using (42), the energy balances in (20) and (22) can be handled by

$$\mathbf{M}_1 \dot{\mathbf{T}}_1 + (\mathbf{N} + \mathbf{O}_1) \mathbf{T}_1 = \mathbf{Q}_{c1}(\mathbf{T}, \mathbf{P}_n), \quad (43a)$$

$$\mathbf{M}_2 \dot{\mathbf{T}}_2 + \mathbf{O}_2 \mathbf{T}_2 = \mathbf{Q}_{c2}(\mathbf{T}, \mathbf{P}_n), \quad (43b)$$

where

$$\mathbf{M}_m = [M^{BA}], \quad M^{BA} = \int_{\Omega^m} \rho c N^A N^B dV, \quad (44a)$$

$$\mathbf{O}_m = [O^{BA}], \quad O^{BA} = \int_{\Omega^m} k \frac{\partial N^A}{\partial x_i} \frac{\partial N^B}{\partial x_i} dV, \quad (44b)$$

$$\mathbf{N} = [N^{BA}], \quad N^{BA} = \int_{\Omega^1} \rho c v_i \frac{\partial N^A}{\partial x_i} N^B dV. \quad (44c)$$

The convection matrix  $\mathbf{N}$  in (44c) is non-symmetric. When this matrix dominates over the symmetric conduction matrix  $\mathbf{O}_1$ , then the thermal solution might be unstable. This might be stabilized by adding artificial conduction along the streamlines by using  $\mathbf{R}\mathbf{T}_1$ , where

$$\mathbf{R} = [R^{BA}], \quad R^{BA} = \bar{k} \int_{\Omega^1} v_i \frac{\partial N^A}{\partial x_i} v_j \frac{\partial N^B}{\partial x_j} dV \quad (45)$$

and  $\bar{k}$  is an artificial conduction coefficient. By inserting the stabilization term  $\mathbf{RT}_1$  into (43a), we obtain the following energy balance for the disc:

$$\mathbf{M}_1 \dot{\mathbf{T}}_1 + (\mathbf{N} + \mathbf{R} + \mathbf{O}_1) \mathbf{T}_1 = \mathbf{Q}_{c1}(\mathbf{T}, \mathbf{P}_n). \quad (46)$$

This equation can also be derived by performing a Petrov-Galerkin discretization, see e.g. the textbook by Donea and Huerta [23].

## 4 Numerical treatment

The equations presented in the previous section are treated sequentially for each time step by decoupling the mechanical and thermal equations. That is, for a given temperature distribution, the mechanical contact problem is first solved, then for the obtained frictional heat distribution the energy balance is solved. Details are presented in this section.

Equations (39) and (40) are put together to form an equation system as

$$\mathbf{h} = \mathbf{h}(\boldsymbol{\eta}) = \mathbf{h}(\mathbf{d}, \mathbf{P}_n, \mathbf{T}) = \mathbf{0}. \quad (47)$$

This is a semi-smooth equation system which is efficiently solved by the following Newton algorithm:

**Newton algorithm:** Let  $\beta = 0.9$ ,  $\gamma = 0.1$  and  $\epsilon$  be a small value. Repeat the following steps:

- 0: Let  $\boldsymbol{\eta}^0$  be a sufficiently good starting point and let  $r = 0$ .
- 1: Find a search direction  $\boldsymbol{\zeta}$  which satisfy

$$\mathbf{h}(\boldsymbol{\eta}^r) + \mathbf{J}(\boldsymbol{\eta}^r) \boldsymbol{\zeta} = \mathbf{0},$$

where the Jacobian  $\mathbf{J}(\boldsymbol{\eta}^r) = \nabla \mathbf{h}(\boldsymbol{\eta}^r)$  when  $\mathbf{h}$  is differentiable. At non-differentiable states the Jacobian is defined by just taking one of the directional derivatives, see Strömberg [14].

- 2: Let  $\alpha = \beta^m$ , where  $m$  is the smallest integer  $0 \leq m \leq 22$  which satisfies the following criterium:

$$\Phi(\boldsymbol{\eta}^r + \beta^m \boldsymbol{\zeta}) \leq (1 - 2\gamma\beta^m) \Phi(\boldsymbol{\eta}^r), \quad \Phi(\boldsymbol{\eta}) = \frac{1}{2} \mathbf{h}^T(\boldsymbol{\eta}) \mathbf{h}(\boldsymbol{\eta}).$$

- 3: Let  $\boldsymbol{\eta}^{r+1} = \boldsymbol{\eta}^r + \alpha \boldsymbol{\zeta}$ .
- 4: If  $\Phi(\boldsymbol{\eta}^{r+1}) \leq \epsilon$ , then terminate with  $\boldsymbol{\eta}^{r+1}$  as an approximate zero of  $\mathbf{h}(\boldsymbol{\eta})$ . Otherwise, update  $r$  with  $r + 1$  and return to step 1.

The time rates appearing in the energy balances are discretized by the trapezoidal rule. Let  $\mathbf{T}^n = \mathbf{T}(t_n)$  at time  $t_n$ , then the temperatures at the next time step  $t_{n+1}$  are updated according to

$$\mathbf{T}^{n+1} = \mathbf{T}^n + \Delta t \left( (1 - \tau) \dot{\mathbf{T}}^n + \tau \dot{\mathbf{T}}^{n+1} \right), \quad (48)$$

where  $\Delta t = t_{n+1} - t_n$ , and  $\tau = 1/2$  (Crank-Nicolson) or  $\tau = 2/3$  (Galerkin). (48) inserted in (46) and (43b) yields

$$\begin{aligned} \left( \mathbf{N} + \mathbf{R} + \mathbf{O}_1 + \frac{1}{\tau \Delta t} \mathbf{M}_1 \right) \mathbf{T}_1^{n+1} &= \mathbf{Q}_1^{\text{eff}} + \mathbf{Q}_{C1}(\mathbf{T}^{n+1}, \mathbf{P}_n^{n+1}), \\ \left( \mathbf{O}_2 + \frac{1}{\tau \Delta t} \mathbf{M}_2 \right) \mathbf{T}_2^{n+1} &= \mathbf{Q}_2^{\text{eff}} + \mathbf{Q}_{C2}(\mathbf{T}^{n+1}, \mathbf{P}_n^{n+1}), \end{aligned} \quad (49)$$

where

$$\mathbf{Q}_m^{\text{eff}} = \frac{(1 - \tau)}{\tau} \mathbf{M}_m \dot{\mathbf{T}}_m^n + \frac{1}{\tau \Delta t} \mathbf{M}_m \mathbf{T}_m^n \quad (50)$$

for  $m = 1, 2$ .

It is also possible to represent (42) in the following way:

$$\mathbf{Q}_{c1}(\mathbf{T}, \mathbf{P}_n) = \mathbf{S}_{P2}(\mathbf{P}_n) \mathbf{T}_2 - \mathbf{S}_{P1}(\mathbf{P}_n) \mathbf{T}_1 + \mathbf{Q}_\mu^1(\mathbf{P}_n), \quad (51a)$$

$$\mathbf{Q}_{c2}(\mathbf{T}, \mathbf{P}_n) = \mathbf{S}_{P1}(\mathbf{P}_n) \mathbf{T}_1 - \mathbf{S}_{P2}(\mathbf{P}_n) \mathbf{T}_2 + \mathbf{Q}_\mu^2(\mathbf{P}_n), \quad (51b)$$

where

$$\mathbf{S}_{Pm} = \mathbf{S}_{Pm}(\mathbf{P}_n) = [\mathbf{S}_{Pm}^A] \quad \mathbf{S}_{Pm}^A = [\mathbf{0} \ [\varphi^0 P_n^A] \ \mathbf{0}] \quad (52)$$

and

$$\mathbf{Q}_\mu^1 = \mathbf{Q}_\mu^1(\mathbf{P}_n) = \xi_\mu^1 \mu \mathbf{P}_n R_{\text{disc}} \omega, \quad (53a)$$

$$\mathbf{Q}_\mu^2 = \mathbf{Q}_\mu^2(\mathbf{P}_n) = (1 - \xi_\mu^1) \mu \mathbf{P}_n R_{\text{disc}} \omega. \quad (53b)$$

Now, (51) and (49) can be formulated compactly as

$$\mathbf{A}(\mathbf{P}_n) \mathbf{T} = \mathbf{Q}(\mathbf{P}_n), \quad (54)$$

where

$$\mathbf{A}(\mathbf{P}_n) = \begin{bmatrix} \mathbf{N} + \mathbf{R} + \mathbf{O}_1 + \frac{\mathbf{M}_1}{\tau \Delta t} + \mathbf{S}_{P1} & -\mathbf{S}_{P2} \\ -\mathbf{S}_{P1} & \mathbf{O}_2 + \frac{\mathbf{M}_2}{\tau \Delta t} + \mathbf{S}_{P2} \end{bmatrix}, \quad (55a)$$

$$\mathbf{Q}(\mathbf{P}_n) = \left\{ \begin{array}{l} \mathbf{Q}_1^{\text{eff}} + \mathbf{Q}_\mu^1 \\ \mathbf{Q}_2^{\text{eff}} + \mathbf{Q}_\mu^2 \end{array} \right\}. \quad (55b)$$

In conclusion, let  $\mathbf{d}^n$ ,  $\mathbf{P}_n^n$ ,  $\mathbf{T}^n$  be given at time  $t_n$ , then  $\mathbf{d}^{n+1}$ ,  $\mathbf{P}_n^{n+1}$ ,  $\mathbf{T}^{n+1}$  are obtained by the following steps:

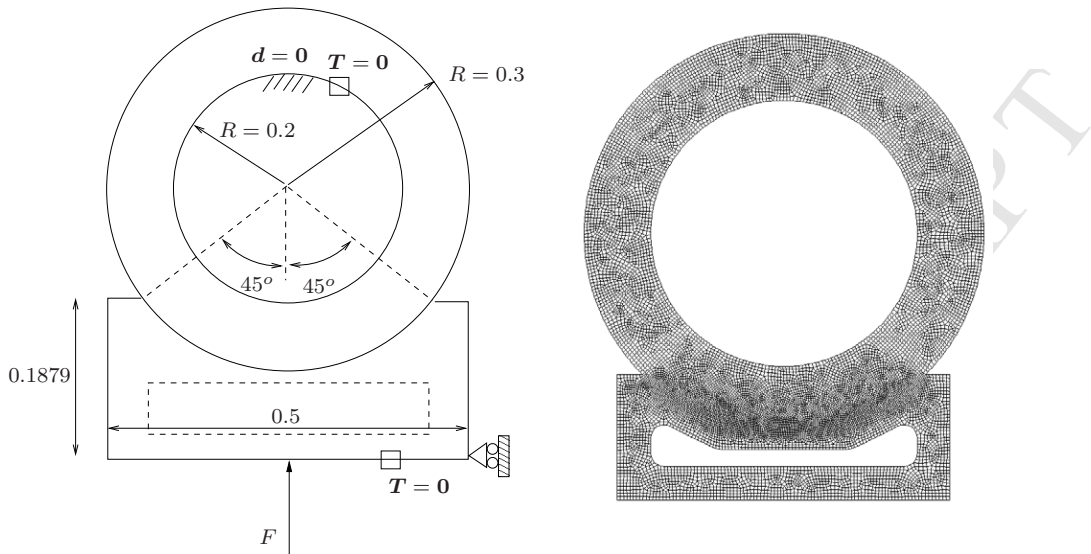


Figure 2: A numerical benchmark with 13353 isoparametric bilinear quadrilateral elements.

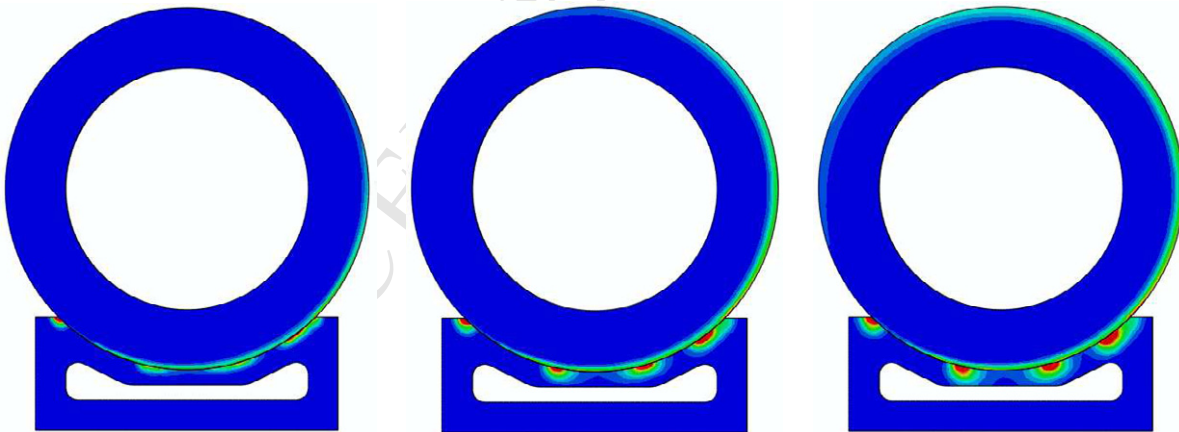


Figure 3: Illustration of the convection during one revolution. The plots are generated after a rotation of  $\pi/2$ ,  $\pi$  and  $3\pi/2$  [rad], respectively.

**Step 1:**

$$\mathbf{h}(\mathbf{d}^{n+1}, \mathbf{P}_n^{n+1}, \mathbf{T}^n) = \mathbf{0}$$

is solved by the Newton algorithm presented previously.

**Step 2:**

$$\mathbf{T}^{n+1} = \mathbf{A}(\mathbf{P}_n^{n+1})^{-1} \mathbf{Q}(\mathbf{P}_n^{n+1}).$$

**Step 3:**

$$\dot{\mathbf{T}}^{n+1} = -\frac{1-\tau}{\tau} \dot{\mathbf{T}}^n + \frac{\mathbf{T}^{n+1} - \mathbf{T}^n}{\tau \Delta t}.$$

Time histories of  $\mathbf{d}$ ,  $\mathbf{P}_n$  and  $\mathbf{T}$  are then generated sequentially by executing the steps above for new time steps  $t^{n+1} = t^n + \Delta t$  ( $n = n + 1$ ). Numerically solutions obtained by this approach are presented in the next section. The time history of  $\mathbf{T}$  from these solutions can then easily be imported to any commercial finite element tool in order to study the thermal stresses more accurately by e.g. performing plasticity analysis with temperature dependent material data. This is a topic of a forthcoming paper.

## 5 Numerical examples

The disc and pad shown in Figure 2 is considered as a numerical benchmark in 2D. Two examples are presented for this benchmark. The dimensions of the pad and the disc are given in meters [m]. The plain strain assumption is adopted with a thickness of 1 [m]. The mesh is also plotted in Figure 2. The disc is meshed using 9867 elements and the number of contact pairs is 189, which is obtained by a finer mesh near the contact surfaces. This is a nice feature with the Eulerian approach. In a Lagrangian approach a finer mesh would have to be used for the whole disc in order to obtain a similar contact discretization. If the finer mesh size is used over the whole disc, then we obtain instead 30583 elements. The pad is meshed with 3486 elements.

Young's modulus is  $2.1\text{E}11$  [Pa], Poisson's ratio is 0.3, the expansion coefficient is  $1.2\text{E}-5$  [1/K], the density is  $7800$  [kg/m<sup>3</sup>], the heat capacity is  $460$  [J/kgK], the conductivity is  $46$  [W/mK] and the conduct conductance is taken to be  $\varphi = 0.1$  [W/NK]. The friction coefficient is set to  $\mu = 0.3$  in both examples and a force of  $F = 20$  [kN] is applied at the center node at the bottom of the pad. The displacements at the bottom of the pad are fixed horizontally and at the inner radius of the disc the displacements are set to zeros. Thus, the motion of the inner radius is only governed by the rigid body rotation. Furthermore, the

temperatures are set to zeros both at the bottom of the pad and at the inner radius of the disc.

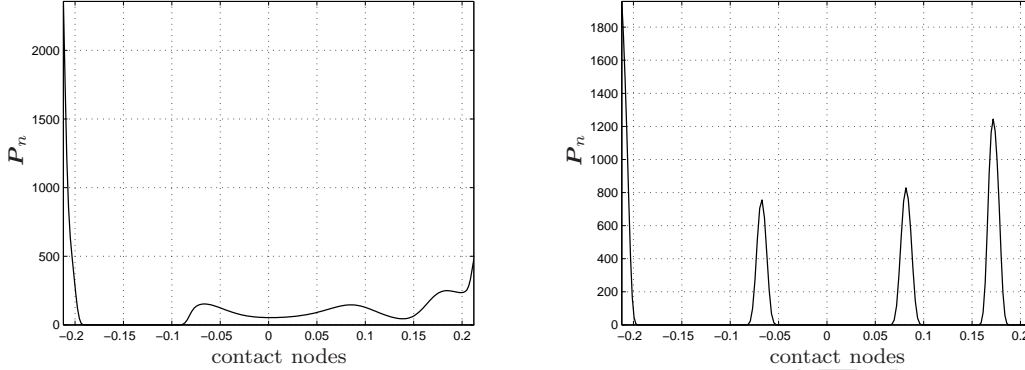


Figure 4: *The normal contact force obtained for zero (left) and non-zero (right) expansion coefficient.*

The first example illustrates the convection in the pad. The benchmark is solved for one revolution. During this revolution the force is applied for 20 increments by using  $\Delta t = 0.25$  [s]. The angular velocity is  $\omega = 2\pi/(20\Delta t)$  [rad/s]. The temperatures are plotted when  $t = 1.25$ , 2.5 and 3.75 [s], see Figure 3. These times correspond to a rotation of  $\pi/2$ ,  $\pi$  and  $3\pi/2$ , respectively. Although the maximum temperature increase is very small, approximately only one degree, it has a tremendous impact on the contact pressure. This is shown in Figure 4, where the contact pressure after 20 time increments is compared to the pressure obtained for zero expansion coefficient. One can see that four hot spots are developed. These will merge together to two hot spots in the next example.

In the second example we present two hot spots obtained for a load history. The force  $F$  is first ramped up by using a log-sigmoid function during 20 increments and then it is held constant for another sixty increments. The angular velocity is 100 [rad/s] and the time step is set to  $\Delta t = 0.5$  [s]. The temperatures at time  $t = 10$ , 20, 30 and 40 [s] are plotted in Figure 5. Two hot spots are developed unsymmetrically on the pad. The asymmetry depends both on the friction force as well as the thermal expansion. If no frictional force is included in the mechanical problem and the expansion coefficient is set to zero, then these hot spot will develop symmetrically instead. The temperatures of the hot spot depend strongly on the contact conductances. This is shown in Figure 6, where the maximum temperature in the pad is given as a func-

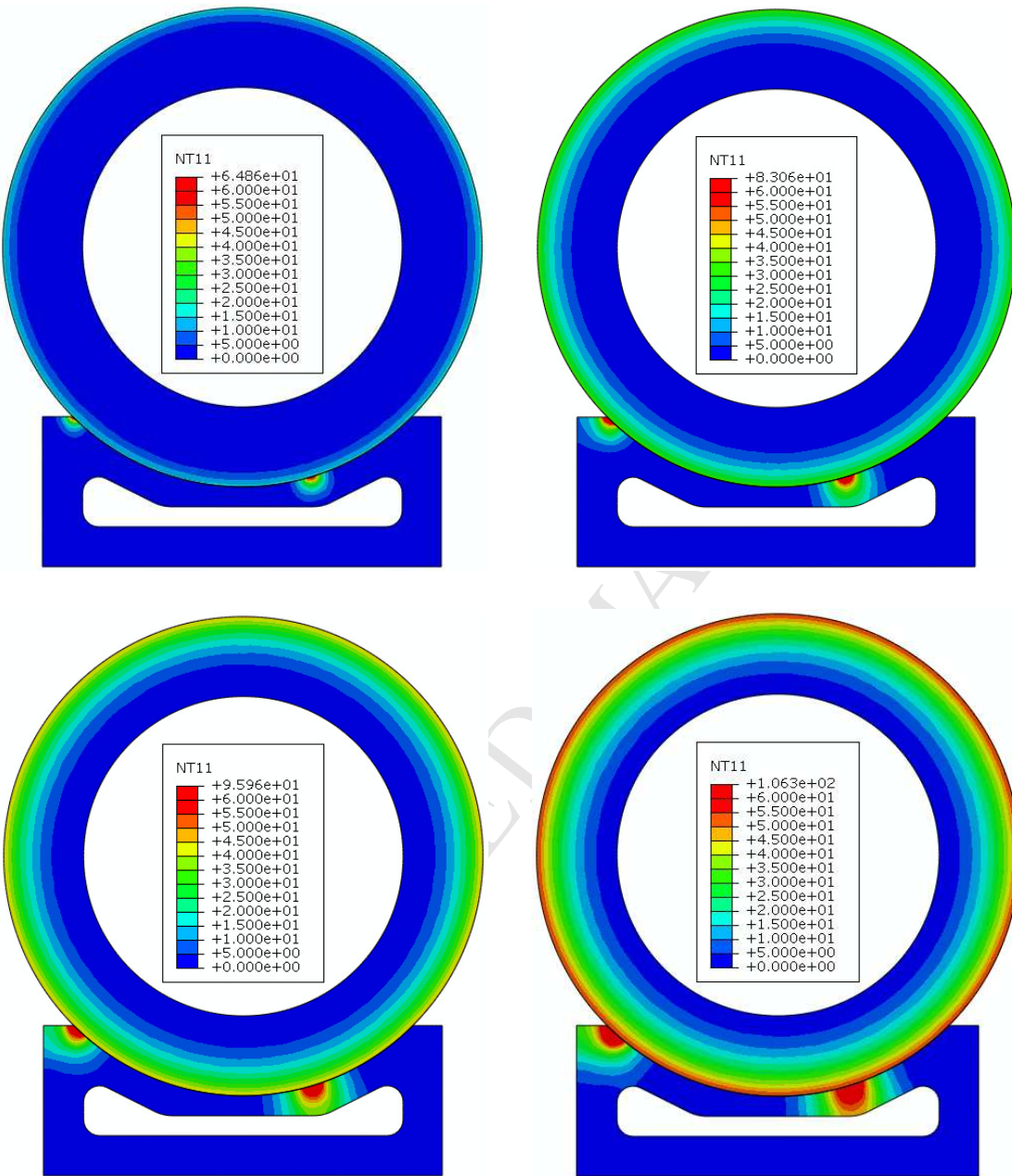


Figure 5: *Development of heat bands and two frictional hot spots during a load history. The CPU-time is 266 [s] on a laptop with an Intel Core i7 2.67 GHz processor.*

tion of the overall contact conductance. For zero contact conductance the maximum temperature in the pad is extremely high, but decreases rapidly for increasing conductance and finally converges towards the maximum temperature of the disc. The behavior of the maximum temperature in the disc is the opposite. Here, the maximum temperature increases slowly with increasing conductance and converges towards the maximum temperature of the pad.

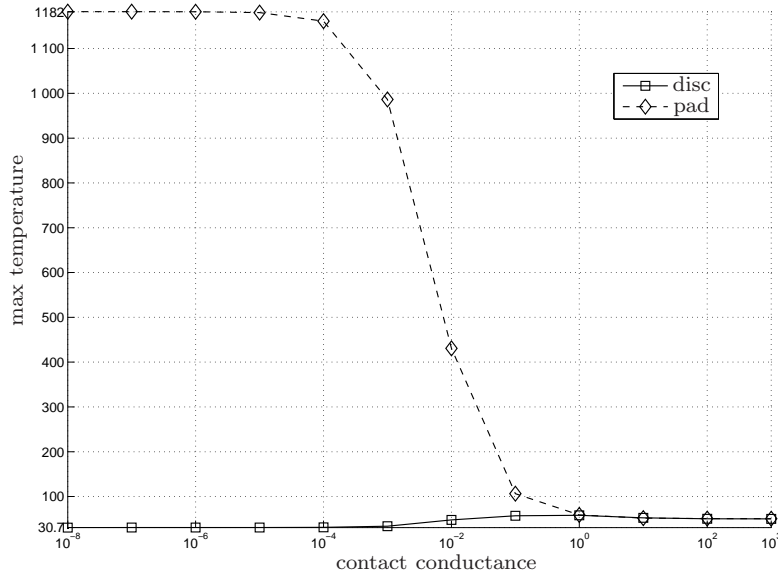


Figure 6: *The maximum temperatures in the disc and the pad as functions of the contact conductance  $\varphi^0$ . The maximum temperature in the pad depends strongly on the contact conductance.*

The bottle-neck of the algorithm is to solve the linear system appearing in the Newton algorithm. Typically 4-7 such linear systems have to be solved for getting convergence in each time step. The system is also non-symmetric due to the friction force and a LU solver must be used. One approach to speed up these calculations is to assume that the friction force has a little influence on the thermal solution<sup>3</sup>. If the friction force is neglected in the mechanical problem, then only 2-3 Newton steps are needed and the linear system also becomes symmetric by inserting (39) into (40) and normalizing (39) by  $r$ . By adopting this approach, the CPU-time is improved significantly. Now, the CPU-time is 82 [s] instead of 266 [s], which was obtained previously. But

<sup>3</sup>Of course, the frictional dissipation is still included in the energy balance.

most important, the thermal solution  $\mathbf{T}$  is similar to the one obtained previously  $\mathbf{T}^{fric}$  when frictional forces were included. The root mean squared error, defined by

$$\epsilon_{sol} = \sqrt{\frac{1}{n_n} (\mathbf{T} - \mathbf{T}^{fric})^T (\mathbf{T} - \mathbf{T}^{fric})}, \quad (56)$$

becomes  $\epsilon_{sol} = 1.7965$ .

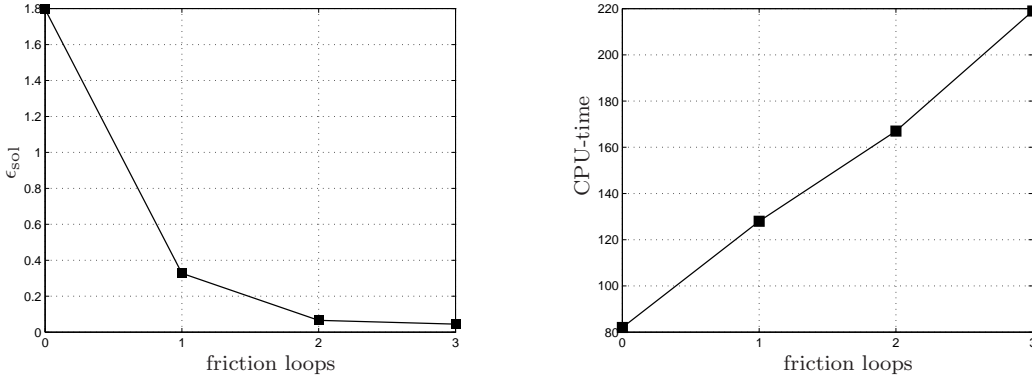


Figure 7: The root mean squared error and CPU-time as functions of extra friction loops.

Another approach for speeding up the calculations but still consider the frictional force is to first solve the frictionless problem and then letting the friction force be defined by the obtained frictionless contact pressure, and solving the friction problem for this constant friction force. That is, at each iteration, (40) is first solved for  $\mu = 0$ . Let  $\hat{\mathbf{P}}_n$  denote the corresponding normal contact force solution and then solve

$$\mathbf{K}_1 \mathbf{d}_1 - \hat{\mathbf{K}}_1 \mathbf{T}_1 + \mathbf{C}_{n1}^T \mathbf{P}_n + \mu \mathbf{C}_{t1}^T \hat{\mathbf{P}}_n = \mathbf{F}_\omega, \quad (57a)$$

$$\mathbf{K}_2 \mathbf{d}_2 - \hat{\mathbf{K}}_2 \mathbf{T}_2 + \mathbf{C}_{n2}^T \mathbf{P}_n + \mu \mathbf{C}_{t2}^T \hat{\mathbf{P}}_n = \mathbf{F}_q. \quad (57b)$$

In general, the number of iterations will be twice the number of iterations for the frictionless case. Of course, in this approach, we will also have a symmetric Jacobian which is most beneficial for large size problems. The CPU-time now becomes 128 [s] and the solution is almost identical to the original one. The root mean squared error is  $\epsilon_{sol} = 0.3272$ , which is small compared to other uncertainties, e.g. the value of the friction coefficient. This approach can of course be applied for several loops. The root mean squared error and CPU-time as functions of extra friction loops are plotted in Figure 7.

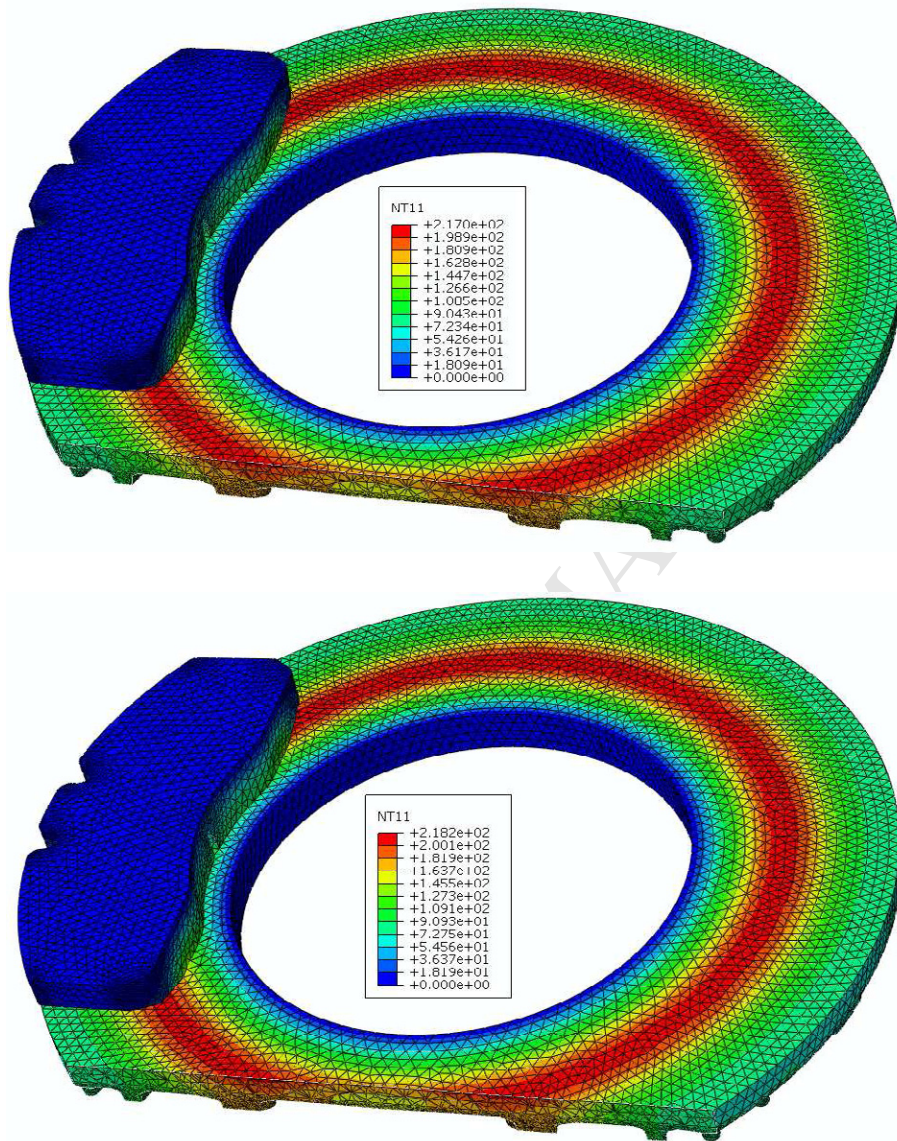


Figure 8: Upper: friction force neglected in the mechanical problem, CPU-time is 2625 [s]. Lower: Simplified friction approach by using one extra friction loop, CPU-time is 4325 [s].

This latter approach is also implemented for the three-dimensional case. This done by using isoparametric 4-noded tetrahedron elements. This is a rational choice which of course might be improved by taking non-linear elements instead. However, an accurate modeling of the global stiffness properties of the complete disc brake system is more important. For instance, a proper modeling of the back-plate of the disc pad is crucial in order to get a good comparison to experimental results. Furthermore, if we instead choice non-linear elements, then the streamline-upwind approach might not be sufficient for stabilizing the thermal equation system. A real disc brake system is solved using this choice of linear elements. The disc is meshed by 393393 elements and for the pad 36007 elements are used. For simplicity, the constitutive parameters are taken to be the same as for the two-dimensional examples. A pad pressure is ramped up for 20 increments by using a log-sigmoid function during 200 [s]. The temperature field is plotted in Figure 8. A heat band clearly appears on the disc. This type of heat bands are also observed in experiments. The total CPU-time is 4325 [s] on a workstation with four Intel Xeon X5450 3.00 GHz processors. The problem is also solved when the frictional force is neglected in the analysis. Almost an identical heat band appears. This is also plotted in Figure 8. The computational time is almost halved. This approach could be very useful when studying new designs for real disc brake systems.

## 6 Conclusions

In this work a method for simulating frictional heating in disc-pad systems is developed and implemented. The key idea of the approach is to use an Eulerian frame for the rotating disc. In such manner, a node-to-node based contact formulation can be adopted, producing most accurate frictional heat solutions at low computational costs. The convective term appearing in this approach is stabilized by the streamline-upwind technique. The method seems most promising. This is shown by solving a two-dimensional benchmark as well as a real disc brake system in 3D. The approach is general and can of course be utilized for other rotating thermo-mechanical systems. In the future, temperature dependency on the material properties should be included. The model could also be extended in several directions, e.g. including wear or considering non-constant angular velocities. **One might also develop the model for non-linear elements. If this is done, then the streamline-upwind technique might fail and one must find more modern Eulerian approaches.** These are examples of topics for

future research.

**Acknowledgement** *The mesh of the three-dimensional disc-pad problem was prepared by Asim Rashid. This project was financed by Vinnova (FFI-Strategic Vehicle Research and Innovation) and Volvo 3P.*

## References

- [1] Strömberg, N., Finite element treatment of two-dimensional thermoelastic wear problems, *Computer Methods in Applied Mechanics and Engineering* (1999) **177**:441–455.
- [2] Ireman, P., Klarbring, A. and Strömberg, N., Finite element algorithms for thermoelastic wear problems, *European Journal of Mechanics, A/Solids* (2002) **21**:423–440.
- [3] Johansson, L. and Klarbring, A., Thermoelastic frictional contact problems: modelling, FE-approximation and numerical realization, *Computer Methods in Applied Mechanics and Engineering* (1993) **105**:181–210.
- [4] Zavarise, G., Wriggers, P., Stein, E. and Schrefler, B.A., Real contact mechanisms and finite element formulation - a coupled thermomechanical approach, *International Journal for Numerical Methods in Engineering* (1992) **35**:767–785.
- [5] Klarbring, A., Lundvall, O. and Strömberg, N., A flexible multi-body approach for frictional contact in spur gears, *Journal of Sound and Vibration* (2004) **278**:479–499.
- [6] Wriggers, P. and Miehe, C., Contact constraints within coupled thermomechanical analysis - a finite element model, *Computer Methods in Applied Mechanics and Engineering* (1994) **113**:301–319.
- [7] Oancea, V.G. and Laursen, T.A., A finite element formulation of thermomechanical rate-dependent frictional sliding, *International Journal for Numerical Methods in Engineering* (1997) **40**:4275–4311.
- [8] Agelet de Saracibar, C., Numerical analysis of coupled thermomechanical frictional contact problems. Computational model and applications, *Archives of Computational Methods in Engineering* (1998) **5**:243–301.

- [9] Rieger, A. and Wriggers, P., Adaptive methods for thermomechanical coupled contact problems, *International Journal for Numerical Methods in Engineering* (2004) **59**:871-894.
- [10] Popp, A., Gitterle, M., Gee, M.W. and Wall, W.A., A dual mortar approach for 3D finite deformation contact with consistent linearization, *International Journal for Numerical Methods in Engineering* (2010) **83**:1428-1465.
- [11] Laursen, T.A., Puso, M.A. and Sanders, J., Mortar contact formulations for deformable-deformable contact: Past contributions and new extensions for enriched and embedded interface formulations, *Computer Methods in Applied Mechanics and Engineering* (2010) in press.
- [12] Hübner, S. and Wohlmuth, B.I., Thermo-mechanical contact problems of non-matching meshes, *Computer Methods in Applied Mechanics and Engineering* (2009) **198**:1338–1350.
- [13] Alart, P. and Curnier, A., A mixed formulation for frictional contact problems prone to Newton like solution methods, *Computer Methods in Applied Mechanics and Engineering* (1991) **92**:353–375.
- [14] Strömberg, N., An augmented Lagrangian method for fretting problems, *European Journal of Mechanics, A/Solids* (1997) **16**:573–593.
- [15] Strömberg, N., Topology optimization of structures with manufacturing and unilateral contact constraints by minimizing an adjustable compliance-volume product, *Structural and Multidisciplinary Optimization* (2010) **42**:341–350.
- [16] Pantuso, D., Bathe, K.J. and Bouzinov, P.A., A finite element procedure for the analysis of thermo-mechanical solids in contact, *Computers & Structures* (2000) **75**:551-573.
- [17] Wauer, J. and Schweizer, B., Dynamics of rotating thermoelastic disks with stationary heat source, *Applied Mathematics and Computation* (2010) **215**:4272-4279.
- [18] Pauk, V.J. and Yevtushenko, A.A., Frictional heating in sliding contact of two thermoelastic bodies, *International Journal of Solids and Structures* (1997) **34**:1505–1516.

- [19] Yevtushenko, A., Ukhanska, O. and Chapovska, R., Friction heat distribution between a stationary pin and a rotating disc, *Wear* (1996) **196**:219-225.
- [20] Laraqia, N., Alilat, N., Garcia de Mariab, J.M. and Bairi, A., Temperature and division of heat in a pin-on-disc frictional device - exact analytical solution, *Wear* (2009) **266**:765-770.
- [21] Nackenhorst, U. The ALE-formulation of bodies in rolling contact, Theoretical foundations and finite element approach, *Computer Methods in Applied Mechanics and Engineering* (2004) **193**:4299–4322.
- [22] Laursen, T.A., On the development of thermodynamically consistent algorithms for thermomechanical frictional contact, *Computer Methods in Applied Mechanics and Engineering* (1999) **177**:274–287.
- [23] Donea, J., and Huerta, A., *Finite element methods for flow problems*, Wiley, (2003).
- [24] Christensen, P., Klarbring, A., Pang, J. and Strömberg, N., Formulation and comparison of algorithms for frictional contact problems, *International Journal for Numerical Methods in Engineering* (1998) **42**:145–173.